IHJPAS. 37 (2) 2024
Ibn Al-Haitham Journal for Pure and Applied Sciences
Journal homepage: jih.uobaghdad.edu.iq
PISSN: 1609-4042, EISSN: 2521-3407

Study of Some Physical Properties of the Superconducting Compound PbBa2Ca2Cu3O8+δ

Fouad Waheed Ali [1*] and Kareem Ali Jasim [2]
[1,2] Department of Physics, College of Education for Pure Sciences (Ibn Al-Haitham), University of Baghdad, Baghdad, Iraq.
*Corresponding Author.

Received: 5 March 2023 Accepted: 10 April 2023 Published: 20 April 2024

doi.org/10.30526/37.2.3309

Abstract

To analyze the structural properties of the $PbBa_2Ca_2Cu_3O_{8+\delta}$ sample, an X-ray diffraction analyzer was used. The results showed that the compound has a tetragonal crystal structure. The crystal lattice constants (a, b, and c) were calculated based on the crystal lattice properties. The crystal size was calculated by four different methods (Scherrer, Williamson-Hall, Halder-Wagner, and size-strain plot), and the best result of C. S = 88.49 nm was for the Halder-Wagner method among other methods. The titration method was used for the samples to find out the percentages of oxygen content (δ). It was found that the oxygen content was (δ = 0.279). Four probes method was used to determine the transition temperature, and it was found that the transition is ($T_{(onset)}$ =138K) The electrical resistance starts with a strong gradient and becomes zero at the critical temperature ($T_{(offset)}$=110K) using Lee's disk method. The results showed that the thermal conductivity of the sample decreases with increasing temperature, as the sample is characterized by a phase ($PbBa_2Ca_2Cu_3O_{8+\delta}$) with a thermal curve. The thermal conductivity starts at (0.12197) for (313K), and the curve decreases at (0.104288) for (553K). The LCR meter device in the range of (50 Hz) to (1 MHz) at room temperature to calculate the dielectric properties of the sample, which include the real dielectric constant (3.58758) and imaginary dielectric constant (10.1710) at frequency (50 Hz), the value of the dielectric constant (real and imaginary) (0.08099, 0.00758) at frequency (1 MHz), and an increase in alternating conductivity values (4.8667*10-7) when the frequency is increased to (1 MHz). One of the most important applications of magnetic resonance imaging is high-speed trains and some modern communication devices.

Keywords: High-temperature, superconductors, Scherrer, Halder-Wagner, Electrical Resistance.

1. Introduction

Superconductivity occurs in a wide variety of materials, including simple elements and some semiconductors doped with a high percentage of impurities, various types of metal alloys, and some specific ceramic compounds whose components are copper and oxygen.

It is well known that there is much interest in high-conducting compounds that have the chemical formula (PbBa2Can-1CunO2n+2+δ) (n = 1, 2, 3, - 8, where n are the Cu-O layers), and the phases of this series have a high transition temperature (Tc), and the transition temperature increases from (94–140 K) under high [4]. Some polycrystalline compounds based on lead have a perovskite structure for the cell unit [5]. The structure of lead-based superconducting materials is as same as that of monolayer copper oxide-based superconductors, where the oxygen atoms are bonded very slightly to the lead layer (Pb-O), and the occupancy sites for elemental lead. are likely to vary greatly depending on the method. The preparation of the compound is the sintering temperature and the sintering time. There are different numbers of homogeneous chains, where Cu-O layers are responsible for superconductivity at high temperatures [6,7]. Highly external conditions, especially the phase (Pb-1223), as some chemical elements occur in a positive exchange with other chemical elements that lead to obtaining superconducting phases with high phase (Pb-1223), which improved the properties of the compound such as critical current density [8-10].

In this research, some physical properties of the superconducting compound (PbBa2Ca2Cu3O8+δ), which include studying the structural properties to obtain the type of the compound and determining the crystal size using four different methods, as well as determining the transition temperature by using continuous electrical conductivity, in addition to studying the dielectric properties of the compound.

2. Materials and Methods

Using the solid-state method to prepare the $PbBa_2Ca_2Cu_3O_{8+\delta}$ superconducting compound, special oxides were prepared from lead oxide (PbO), barium oxide (BaO), copper oxide (CuO), and calcium oxide (CaO), high-purity materials from global and American-origin sources (BASF). The oxides were inside a closed oven at a temperature of 250 °C and a time of 60 minutes to get rid of the moisture content. They were then cooled, and then the weights of the oxides were taken for the PbBa2Ca2Cu3O8+δ compound according to equation (1) [9]:

$$PbO + 2BaO + 2CaO + 3CuO \rightarrow PbBa_2Ca_2Cu_3O_{8+\delta} \quad (1)$$

The oxides were weighed according to their concentration inside the compound using a sensitive scale (Metter H35, AR) with an accuracy of: 0.0001 and a capacity of (120 gm), then the powders were collected and taken to preparation using the solid-state reaction method, and it was implemented in two steps:

1- Grinding the three powders (Ba-O Cu-O, and Ca-O) using an agate mortar and mixing them with propanol to ensure homogeneous mixing, the mixing process continued for (90 min), and then an electric mixer was used to mix the mixture for (120 min). To obtain a very fine and homogeneous powder, the mixture was calcinated at 500 °C for (60 minutes) and the powder was cooled to room temperature.

2 - The mixture is ground in the first step, and lead oxide (Pb-O) is added. The grinding process continued for two hours to obtain a homogeneous composition of the $PbBa_2Ca_2Cu_3O_{8+\delta}$ compound. After that, the powder is pressed under pressure (7ton/m2) using a diameter meld (1.6 cm) and thickness (0.3 cm), and then the sample is sintered in the form of a disk in a programmed electric oven at a temperature of 850 °C, a sintering time of (120hr), and at a thermal sublimation rate of 5 °C/min.

To study the electrical properties, the four-point probe technique was used to calculate the transition

temperature (Tc) of superconducting materials by measuring current and voltage (resistance) as a function of temperature according to the source [11].

To analyze the structural properties of the $PbBa_2Ca_2Cu_3O_{8+\delta}$ sample, a Shimadzu-type XRD analyzer (Current: 35mA, Voltage: 40 kV, wavelength: 1.5406A°) at room temperature was used. To reveal the type of crystal structure and calculate the constants of the crystal lattice (a, b, c) by Cohen's method [12, 13] and the proportions of phases using the following mathematical relationship [14]:

$$V_{ph}= \frac{\sum I_0}{\sum I_1+\sum I_2+\sum I_n} * 100\% \quad (2)$$

Where Vph is the ratio of the phase to be calculated I_0 is the intensity of the phase and I_1, I_2, In other d_{hkl} phases included in the chemical composition.

The (d_{hkl}) distance between planes, which can be calculated using the diffraction angle at a peak using Bragg's law [15]:

$$d_{hkl}= n\lambda/2\sin\theta \quad (3)$$

Where d is the spacing between atomic planes in A° unit, θ is Bragg's angle, n is the integral number order, and λ: represents the wavelength of the X-ray (1.540598 Å). For calculating the volume of the sample (V), use this equation [16]:

$$V=a*b*c \quad (4)$$

Calculate the unit cell density (d_m) using the following mathematical relationship [17]:

$$dm = \frac{Wm}{V*Na.} \quad (5)$$

W_m: Molecular weight is measured in units (amu), V: unit cell volume (cm^3), and N_a- Avogadro's number is measured in (particle/gram mol).

Then the full width was calculated at mid-maximum ($\boldsymbol{\beta}_{hkl}$) by using the Origin (2018,32-bit)) program to calculate crystalline size by four different methods (Scherrer-Williamson-Hall, Halder-Wagner, and size-strain plot), and the equations used for all methods in calculating crystal size will be shown:

2.1. Scherrer method

$$C.S = \frac{k\lambda}{\beta_{hkl}\cos\theta} \quad (6)$$

Where: (C.S) - crystal size, K - constant (0.94), λ - represents the wavelength of the X-ray (1.540598 Å), θ represents the diffraction angle, $\boldsymbol{\beta}_{hkl}$: full width at mid-maximum (FWHM) [18].

2.2. Williamson-Hall [19]

$$(\beta_{hkl}\cos\theta) = \left(\frac{k\lambda}{C.S}\right) + \varepsilon\,(4\sin\theta) \quad (7)$$

Where **ε** is the strain.

2.3. Halder-Wagner:

$$\left(\frac{\beta^*_{hkl}}{d^*_{hkl}}\right)^2 = \left(\frac{1}{C.S}\right).\left(\frac{\beta^*_{hkl}}{{d^*_{hkl}}^2}\right) + \left(\frac{\varepsilon}{2}\right)^2 \quad (8)$$

B^*_{hkl}: the broadening reciprocal lattice point (B^*_{hkl} =B cosθ/λ) and d^*_{hkl} : the lattice plane spacing for reciprocal lattice (d^*_{hkl}=2sinθ/λ) [20] .

4-Size-Strain plot (SSP) [21]:

$$(d_{hkl}.\beta_{hkl}.\cos\theta)^2 = \left(\frac{k\lambda}{C.S}\right)({d_{hkl}}^2.\beta_{hkl}.\cos\theta) + \left(\frac{\varepsilon^2}{4}\right) \quad (9)$$

The values of the thermal conductivity coefficient of the samples (K) are calculated after measuring the thickness of the sample (ds) and radius (r) by equation (8) [22, 23]:-

$$K\left(\frac{TB-TA}{ds}\right) = e\left[T_A + \frac{2}{r}\left(dA+\frac{1}{4}ds\right) T_A+\frac{dsTB}{2r}\right] \quad (10)$$

Where d_s, d_A, d_B, *and* d_C*:* are thicknesses of the sample, disks *A, B, C (mm),* T_A, T_B, *and* T_c*:* are temperatures of the disks *A, B, and C* (℃) and *e* : heat loss in (sec/cm^2), as shown in **Figure 1**.

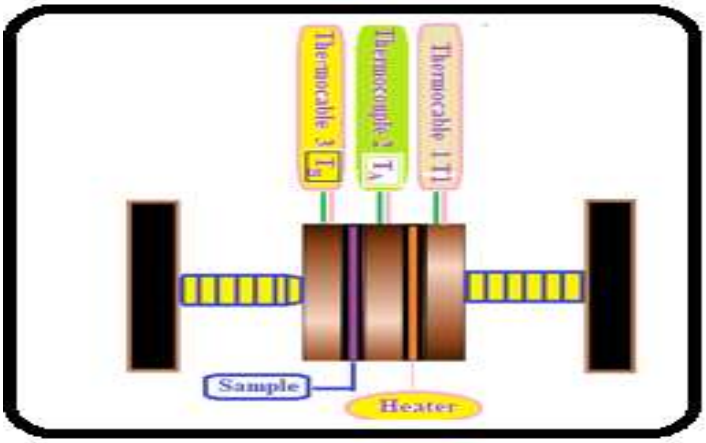

Figure 1. diagram of Lee's disk

While the sample Dielectric properties, which include ,Dielectric constant (Real and Imaginary) loss tangent factor, and alternating electrical conductivity, were studied as a function of frequency in the range (50 Hz to 1 MHz) at room temperature, according to the following equations [24].

$$\dot{\varepsilon}=Cd/A\epsilon_o \quad (11)$$

$$\tan\delta=\ddot{\varepsilon}/\dot{\varepsilon} \quad (12)$$

$$\sigma_{(a.c)}=2\pi f\epsilon_o\ddot{\varepsilon} \quad (13)$$

Where: C represents the capacitance (Farad), d is the sample thickness (m), A represents the area of the electrodes (m2), $\varepsilon_\circ$ is the permittivity of a vacuum (8.85 x 10-12 F/m), and f is the frequency (Hz).

3. Results

3.1 XRD Results

The samples were examined using an X-ray diffraction analysis to estimate the data related to the crystal structure. The X-ray diffraction analysis data is shown in **Figure 2.**, which revealed that the ($PbBa_2Ca_2Cu_3O_{8+\delta}$ compound) consists of almost three dominant phases. The diagram shows of the 1223-phase, which represents the high phase as the dominant phase, with percentages of the lower phases 1201 ($PbBa_2CuO_{4+\delta}$ compound) and 1212 ($PbBa_2CaCu_2O_{6+\delta}$ compound) and some impurities at the end of the diagram, and the reason for the presence of more than two phases can be linked to the accumulation of atoms of different elements along the axis [23]. There is a separation between phases, and some of them turn into a more stable phase, in addition to the method of preparation by solid reaction, which rarely produces a single phase, so in most cases it includes multiple phases, but the concentration of the dominant phase requires regular control of the preparation conditions and other variables that play a major role in the production of the phase singular [25, 26]. The increase in phase concentration (Pb-1223) may be attributed to the introduction of (Cu-O) layers between the phase layers (Pb-1212), which leads to an increase in phase ratio (Pb-1223).

Figure 2. shows the high phase (H) and the low phase (L), represented by the $PbBa_2Ca_2Cu_3O_{8+\delta}$ compound, and the low phase represented by 1201 ($PbBa_2CuO_{4+\delta}$) and 1212 ($PbBa_2CaCu_2O_{6+\delta}$),

where the phase ratios calculated mathematically using equation (2) by means of angular positions. Diffraction (2θ) and intensity (I) for each phase were the ratio of the high phase (81.22%) and the low phase (18.78%). The reason for the difference in the ratio of the high and low phases of the superconducting compound in this model is a change in the ratios of oxygen content, displacement in the atomic structure. The regularity ratios of positive ions that affect the stacking between atoms along the c axis [27] showed that the structure of the compound ($PbBa_2Ca_2Cu_3O_{8+\delta}$) is a tetragonal polycrystalline structure, and the oxygen content ratio (δ) was calculated. It was (0.279), which has a significant effect on the introduction of layers of (Cu-O) and (Ca-O) into the crystal structure of the $PbBa_2Ca_2Cu_3O_{8+\delta}$ compound. As for the unit cell density (dm), its value was (6.224), and the cell unit volume (V) is equal to ($407.65A^3$). As shown in **Table 1.**

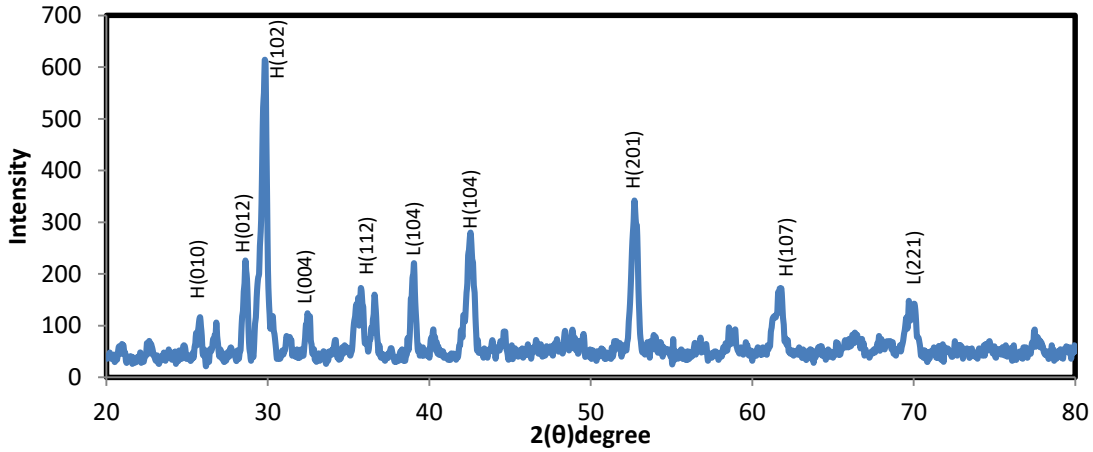

Figure 2. Represents the X-ray diffraction (XRD) of the HgBa2Ca2Cu3O8+δ sample

Table 1. values of the lattice constants (a, b, c), phase ratios (Vph%), ratio (c/a), theoretical density (dm), and oxygen content ratios (δ) of the $PbBa_2Ca_2Cu_3O_{8+\delta}$(Pb-1223)sample

Sample	a(A°)	b(A°)	c (A°)	a/c	V (A°)3	d_m	δ	$V_{ph(H)\%}$	$V_{ph\ (L)\%}$
Pb-1223	3.842	3.8414	27.62	0.139	407.66	6.224	0.279	81.22	18.78

3.2 Calculating the crystal size

The crystal size of the sample ($PbBa_2Ca_2Cu_3O_{8+\delta}$) Was calculated four different methods and To obtain the best crystal size by calculating the value of (R^2), which is a statistical measure to find out how close the data is to the appropriate regression line for it in the graph within the Mat Lab program, also To know the coefficient of determination, or multiple regression coefficient of determination. The R-squared is used to determine the reliability of the correlation between the variables for the (X) and (Y) axes, its value ranges from (+1 to -1). If the value of ($R^2 > 0.7$), this value is generally considered to have a strong effect size and high accuracy, but if the value of ($R^2 < 0.5$), this value is generally considered to have a weak effect size or low accuracy.

1. Scherrer equation

Figure 3, shows the relationship between (cosθ) and ($1/\beta_{(hkl)}$) by using the Scherrer equation to find the crystal size, which was calculated from the slope of the curve according to the slope equation (y=0.0035x+0.367) it was found that it is equal to (41.36nm) and ($R^2 = 0.7599$) as shown in **Figure 3**.

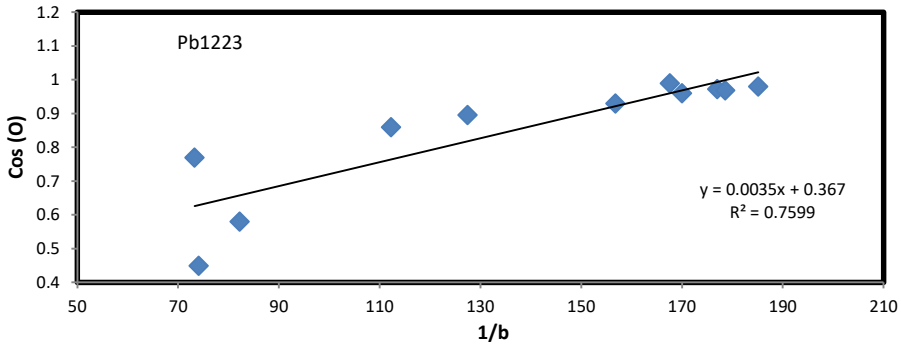

Figure 3. Represents the calculation of the crystal size of the model ($PbBa_2Ca_2Cu_3O_{8+\delta}$) by Scherrer method

2. Williamson-Hall equation

After determining each of the values of the full width at half maximum B_{hkl} (FWHM) and sinθ, cosθ for each vertex by using **Figure 2.** Equation No. 7 was used, which represents the Williamson-Hall method, and then **Figure 4,** was drawn, which represents the relationship between two axes (4sinθ) and (B cosθ) to calculate the slope of equation (y=0.0033x +0.00329) of the straight line to determine the strain (ε), it was found that it is equal to (0.0033). As for the intersection of the straight line with the y-axis, which represents ($\frac{k\lambda}{C.S}$) from Equation 7, we extracted the crystal size (c.s), to be (44nm), the precision modulus is (R^2 = 0.2174).

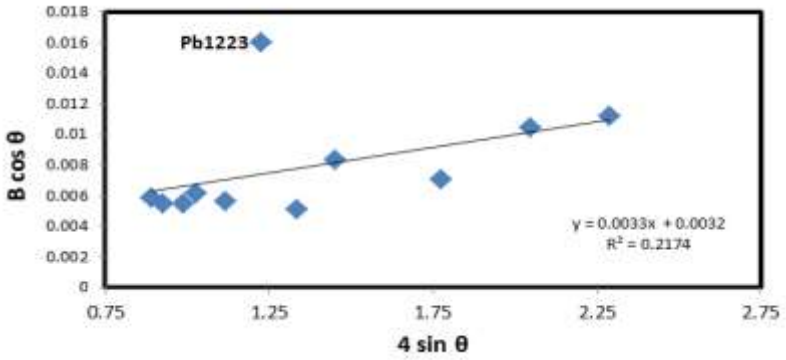

Figure 4. The calculation of the crystal size of the sample (PbBa2Ca2Cu3O8+δ) by the Williamson-Hall method

3. Halder-Wagner method

To calculate the crystal size by the Halder-Wagner method, the crystal size was determined according to Equation (8) by drawing the relationship between $(B_{hkl}* / d_{hkl}*)^2$ and $(B*_{hkl}/d_{hkl}{}^2*)$ in **Figure 5**. The slope of the straight line was determined by the equation ($y=0.0113x-3*10^{-5}$), where the crystalline size was extracted from the slope of the straight line (1/0.0113) to be (88.49nm). The strain value can be calculated from the intersection of the straight line with the y-axis and the result showed that it is equal to (0.010) and the accuracy factor (R^2 = 0.9891), as shown in **Figure 5**.

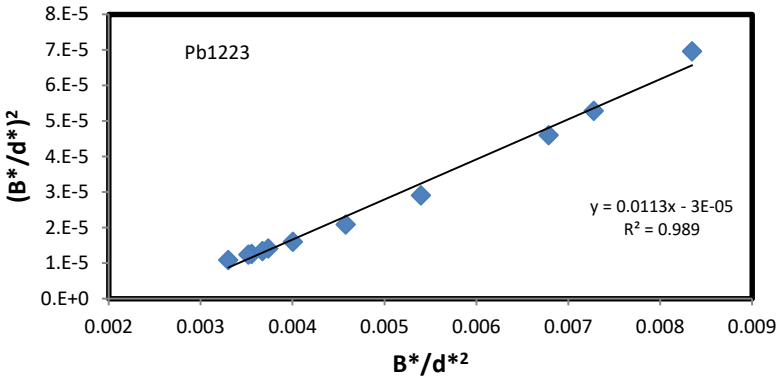

Figure 5. The calculation of the crystal size of the model (PbBa2Ca2Cu3O8+δ) by the Halder-Wagner method

4.Size-strain plot method

Calculate crystal size by SSP (size-strain plot), the crystal size is determined according to Equation No. (9) by plotting the relationship between (d_{hkl}^2.B_{hkl}.cosθ) and (d_{hkl}. B_{hkl}. cosθ)^2 in **Figure 6**. The crystal size was extracted from the slope of the straight line of equation (y=0.0041x-0.0001) and the strain value from the intersection of the straight line with the y-axis. The result showed the crystal size of the sample (Pb 1223) is (35.30 nm), the coefficient of specificity or accuracy (0.7347) and the strain value (0.020).

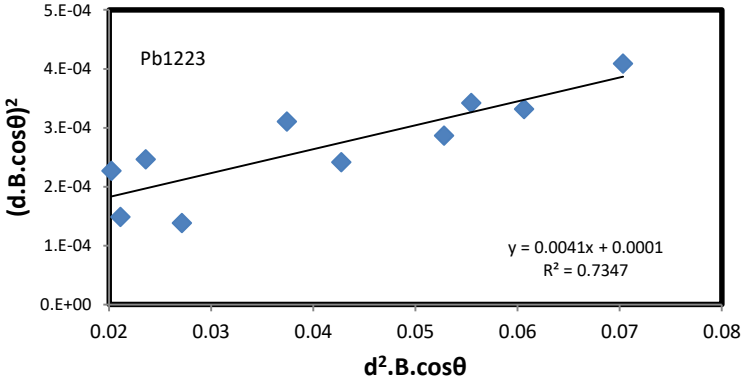

Figure 6. Calculation of the crystal size of the sample ($PbBa_2Ca_2Cu_3O_{8+\delta}$) by (SSP) method

Table 2, displays the calculation of the crystalline size and accuracy coefficient (R^2) of samples of ($PbBa_2Ca_2Cu_3O_{8+\delta}$), using four distinct methods where the results showed that there is a discrepancy in the values of crystal size calculated by these four methods because each of these methods depends mainly on the width of the X-ray diffraction analysis peaks. And the accuracy scale of the results depends on the factor R^2, the closer its value is to one in a certain way, the optimal method for the measured sample [20, 26, 27]. Since the Halder-Wagner method in our results gave R^2=0.9890, so the optimal method for calculating the crystal size in this study is the Halder-Wagner method, where the crystal size was (C. S=88.49 nm) and the strain=0.010 as shown in **Table 2 .**

Table 2. Results of calculating the crystalline size, strain and (R^2) for the $PbBa_2Ca_2Cu_3O_{8+\delta}$ samples

Method	Crystalline size nm	strain	R^2
Scherrer	41.36	------	0.7599
Williamson-Hal	44.0	0.0033	0.2174
Halder-Wagner	88.94	0.010	0.9891
SSP	35.30	0.020	0.7347

3.3 Electrical conductivity

The Electrical resistance was measured as a function of the temperature of the samples using the four-point probe technique by measuring the voltage applied to the sample, the current passing through it, and the temperature of the sample while it was cooled using liquid nitrogen. The relationship between electrical resistance and temperature is depicted in **Figure 7**. The Figure shows the relationship between electrical resistance and temperature changed in the range of (77 to300) K. It is noted through this sample that the electrical resistance (ρ) has a metallic behaviour as it decreases with increasing temperature [28]. It is also noted that this drop in resistance (ρ) becomes almost sharp at a certain temperature called the initial transition temperature ($Tc_{(onset)}$) and then becomes zero at the transition temperature ($Tc_{(offset)}$) where it was found that the (critical) transition temperature ($Tc_{(onset)}$ =138K) where the electrical resistance starts with a strong gradient and becomes zero at the critical temperature ($Tc_{(offset)}$=110K). The width of the transition temperature (ΔTc) is (28K). It is clear that this sample also shows a small scale in the width of the transition temperature (ΔTc), which tends to decrease due to the multiphase superconductivity in the sample. In addition to the role of oxygen, the concentration of chemical elements in the samples plays a major role at the expense of critical temperature [25, 29, 30, 31].

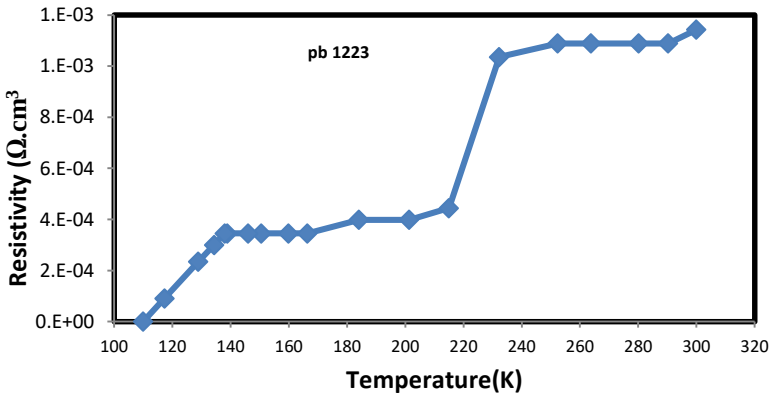

Figure 7. Transition temperature of the superconducting compound ($PbBa_2Ca_2Cu_3O_{8+\delta}$)

3.4 Thermal Conductivity Behavior

The values of the thermal conductivity coefficient of the ($PbBa_2Ca_2Cu_3O_{8+\delta}$) (K) is calculated after measuring the thickness of the sample (0.3mm) and radius (1.6 cm) by applying equation (10). The thermal conductivity for different temperatures is shown in **Figure 8**, which represents the relationship between the thermal conductivity as a function of temperature. The curve shows that

the results of the thermal conductivity of the sample decreases with increasing temperature, as the sample is characterized by phase ($PbBa_2Ca_2Cu_3O_{8+\delta}$) with a thermal curve. Thermal conductivity starts at (0.12197) at (313K) temperature and the curve decreases at (0.104288) at (553K) temperature. It was found that the thermal conductivity decreases with increasing the temperature. This behavior is influenced by the quality and quantity of the chemical elements included in the sample .Thermal conduction is one of the most important ways of transferring heat within or between solid bodies upon thermal contact. The thermal conductivity of the sample ($PbBa_2Ca_2Cu_3O_{8+\delta}$) represents the transfer of heat from hotter to cooler particles under Fourier's law of macroscopic inertia. the compound ($PbBa_2Ca_2Cu_3O_{8+\delta}$) depends on the structure of the substance, the chemical composition, and the type of bond between them, and heat is transferred by means of phonons. The higher the thermal conductivity of the compound, the more perfect the crystal structure, the greater the mineral impurities, the more deformable the crystal lattice, and the lower the thermal conductivity. Also, the occurrence of this deformation in the metal structure reduces the thermal conductivity, which gradually decreases with increasing temperature as shown in **Figure 8.** [32, 33].

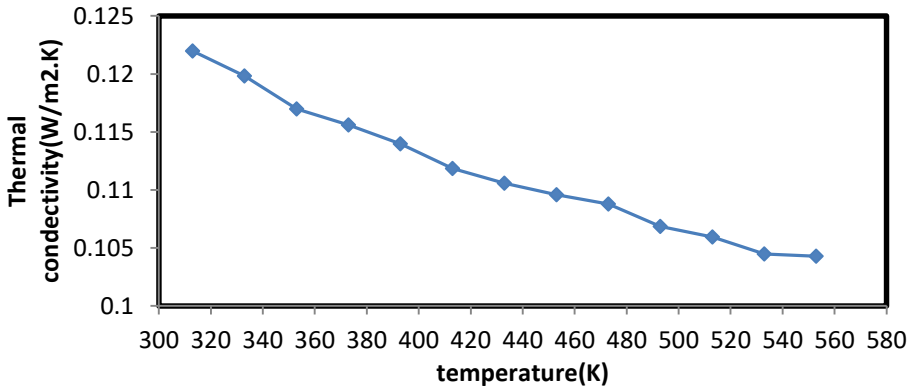

Figure 8. Thermal conductivity as a function of the temperature of the sample($PbBa_2Ca_2Cu_3O_{8+\delta}$)

3.5 Dielectric properties

To calculate the insulating properties of the sample ($PbBa_2Ca_2Cu_3O_{8+\delta}$), the (LCR meter) was used In the frequency range of (1MHz-50Hz). the real dielectric constant (έ), the imaginary dielectric constant (ε̆), the dielectric loss tangent (tanϭ), and the alternating electrical conductivity (ϭa.c) were calculated. It was found that the real dielectric constant is (3.58758) and the imaginary dielectric constant is (10.1710) at frequency (50Hz), and the values of the dielectric constant (real and imaginary) (0.08099, 0.00758) are at frequency (1MHz), and this indicates the amount of decrease of the real dielectric constant when the frequency is increased [34,35], as shown in **Figures 9** and **10**.

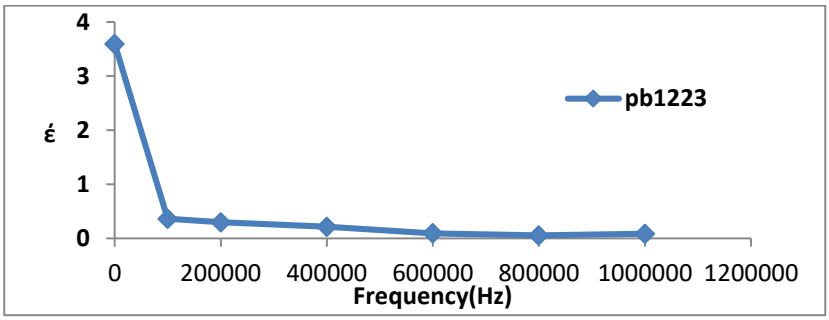

Figure 9. Diagram of the real dielectric constant of a compound (PbBa2Ca2Cu3O8+δ)

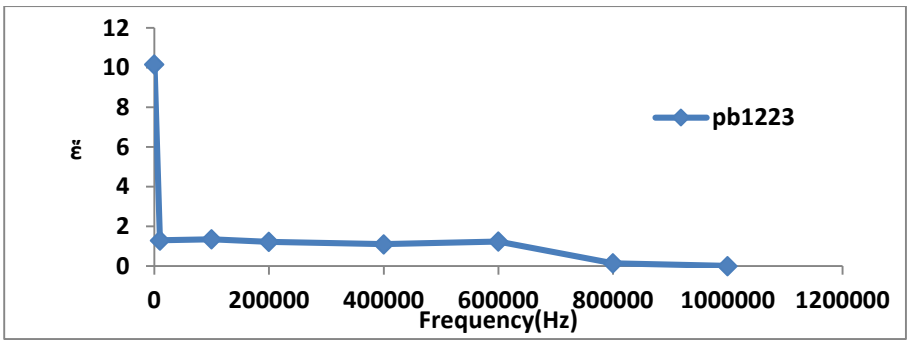

Figure 10. Diagram of the imaginary dielectric constant of a compound (PbBa2Ca2Cu3O8+δ)

It is also noted that there is a decrease in the values of the dielectric tangent with increasing frequency, where it begins to decrease from (2.83508) to (0.935923) with increasing frequency. this is due to the role of polarization, as the total polarization (rotational, electronic, and ionic) operates at frequencies less than 10,000 Hz, while the electronic polarization remains operating at higher frequencies, which leads to an increase in alternating conductivity values ($4.8667*10^{-7}$) when the frequency is increased to (1MHz) [35,36] as shown in **Figures 11, 12** and **Table 4**.

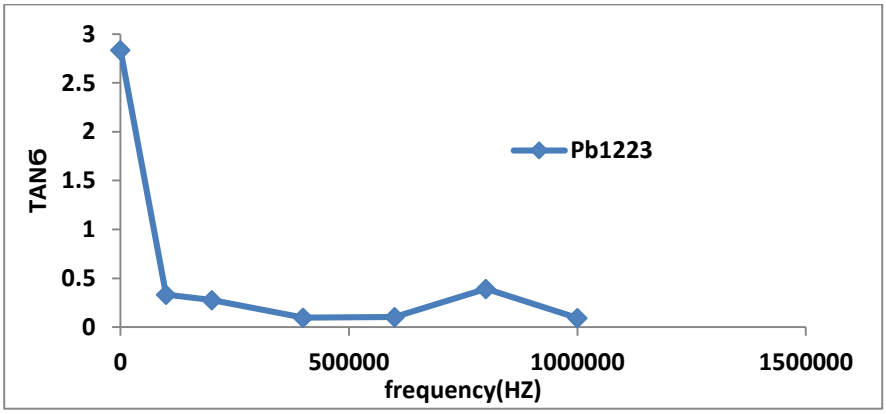

Figure 11. Diagram of the dielectric loss constant of a compound ($PbBa_2Ca_2Cu_3O_{8+\delta}$)

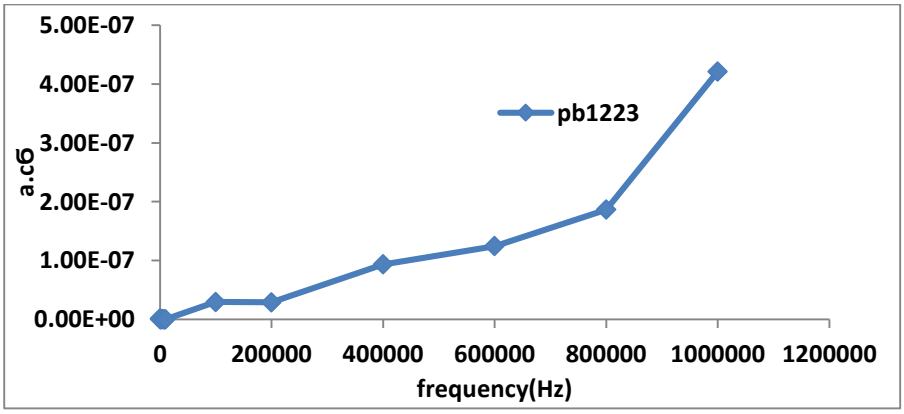

Figure 12. Diagram of the alternating electrical conductivity of a compound ($PbBa_2Ca_2Cu_3O_{8+\delta}$)

Table 4. Represents the values of the dielectric properties of the compound (PbBa2Ca2Cu3O8+δ) for a range of frequencies from (50Hz-1MHz)

Sample(pb1223)	50 Hz	1MHz
έ	3.58758	0.08999
ε̋	10.17108	0.007581
tanϭ	2.83508	0.935923
ϭa.c	$1.4489*10^{-7}$	$4.8667*10^{-7}$

5. Conclusions

In this work, the superconducting properties of the sample ($PbBa_2Ca_2Cu_3O_{8+\delta}$) were fabricated, checked, and calculated. This sample mainly contains several phases with different proportions of Pb-1212, pb1201, and Pb-1223, and according to the observations in the sample, X-ray diffraction (XRD) examination revealed that.the structure of the compound ($PbBa2Ca2Cu3O_{8+\delta}$) is a polycrystalline structure of the tetragonal type, and the percentage of oxygen content was calculated ($\delta = 0.279$), which has a significant effect on the introduction of layers of CuO and CaO into the crystal structure of the compound ($PbBa_2Ca_2Cu_3O_{8+\delta}$). The crystalline size and precision coefficient (R^2) of the compound ($PbBa_2Ca_2Cu_3O_{8+\delta}$) were calculated by means of four distinct methods in the research. The results showed that the optimal method for calculating the crystalline size of the sample ($PbBa_2Ca_2Cu_3O_{8+\delta}$) is the Halder-Wagnes method. (Halder-Wagner), where the crystal size was (C.S= 88.94 nm) with a specificity factor (R^2=0.9891), and a strain of (0.010). It was revealed that the sample of the compound (Pb-1223) has metallic behaviour and a transition temperature ($Tc_{(onset)}$=138K) at which the electrical resistance begins to decrease with a strong gradient and then becomes (zero) at the critical temperature ($Tc_{(offset)}$=110K) and the transition temperature (ΔTc) is (28K). The thermal conductivity of the compound ($PbBa_2Ca_2Cu_3O_{8+\delta}$) was examined. It is noted that thermal conductivity decreases with increasing temperature. On the other hand, the results showed that the thermal conductivity of the sample decreases whenever the temperature is applied as the sample is characterized by the phase (pb-1223) with a thermal curve that begins to show the thermal conductivity at (0.12197) at (313K), and the end of the curve is (0.104288) at (553K) since the sample (1223).and found that the real dielectric constant is (3.58758) and the imaginary dielectric constant is (10.1710) at frequency (50 Hz), the values of the dielectric constant (real and imaginary) (0.08099, 0.00758) are at frequency (1 MHz), and there is an increase in alternating conductivity values ($4.8667*10^{-7}$) when the frequency is increased to (1 MHz).

Acknowledgement

I extend my thanks to the College of Education for pure science Ibn Al-Haitham, University of Baghdad for assisting in completing this work by opening private laboratories and providing scientific facilities by the staff of the Physics Department to help support the research project.

Conflict of Interest

The authors declare that they have no conflicts of interest.

Funding: None.

References

1. Li Substitution on Bi2-x LixPb0.3Sr2Ca2Cu3O10+ δ compound. *Ph.D. thesis* , Roofs, N. Q.; The Impact of Preparation Condition *university of Baghdad college of science* **2014**, *12*, 23-34. http://dx.doi.org/10.4236/msa.2015.64036
2. Kittel, C., Introduction to solid state physics, *4th ed, John Wiley and sons* **1971,** *23*, 233-245.
3. Omar, M. A. Elementary solid state physics. *5th ed., Addis ion-Wesley* **1993**, *12*, 123-134.
4. Malandrin, G.; Perdicaro, L.M.S.; Cassinese, A.; Prigiobbo, A. MOCVD growth, micro-structural, and superconducting properties of a-axis oriented TlBaCaCuO thin films. *Physic* **2004,** *894*, 408 –410. https://doi.org/10.1021/CM034979%2B
5. Lao, J. L.; Wang, J. H.; Wang, D. Z.; Tu, Y.; Yang, S. X.; Wu, H. L. *Physical Appl* **2000**, *333*, 221-228. DOI: 10.3390/ijms161125942
6. Sastry, P. V.; West, A. R.; *Physical Appl* **1995,** *250(87)*, 23-45.
7. Li, Y. F.; Chmaissem, Z. Z.; *Sheng Physica* **1995,** *248*, 42-54.
8. Torardi, C. C.; Subramanian, M. A.; Calabrese, J. C.; Gopolakrishnan, J.; Morrissey, K. J.; Askew, T. R.; Flippen, R. B.; Chowdhry, U.; Sleight, A. W.; *Science Appl* **1988**, *240*, 631.
9. Jasim, K. A.The effect of simultaneous doping of Pb in Tl-O_δ layer of Tl1-xPbx Ba2Ca2Cu3O9- δ, *Ibn Al-Haitham Journal for pure and applied sciences* **2008**, *23(3)*, 34-45. https://doi.org/10.1016/j.egypro.2018.11.183
10. Jasim, K. A.Effect of Pressure on The Structural and Electrical Characteristics of Tl0.8Sb0.2Sr2Ca2Cu3O9-δ Superconductors Prepared by Solid State Reaction Technique. *Materials Science & Technology Conference and Exhibition (MS&T'09) Pittsburgh Pennsylvania, U.S.A*, **2009,** *4*, 23-33. DOI:10.13140/RG.2.2.24079.94885
11. Satish, K.; Hussain, M.; zulfequar, M.; *physical Appl* **2006,** 371, 193. https://doi.org/10.1016/j.physb.2006.04.036
12. Jasim, K. A. Superconducting Properties of Hg0.8Cu0.15Sb0.05Ba2Ca2Cu3O8+δ Ceramic with Controlling Sintering Conditions, *J. Supercond Nov Magn, Journal of superconductivity and novel magnetism* **2012,** *25(6)*, 1713-1717. https://doi.org/10.1007/S10948-012-1507-3
13. Che, G. C.; Du, Y. K.; Wu, F.; Zhao, Z. X. Solid state Commune **1994**, *89* (*11)*, 903-912.
14. Myers, H. P.; Introductory Solid State Physics, *2nd ,Taylor & Froncies* **1997**, *12(3)*, 34-39.
15. Nguyen, E. T.; Sierra, D. Eguiraun, H.; Lizundia, E.; Iridescent cellulose nanocrystal Films : The link between structure colour and Bragg**'**s law, *Eur. J. phys* **2018,** *39(4)*, 45-52.
16. Uesugi, T.; Higashi, K. First-principles studies on lattice constant and local lattice distortions in solid solution aluminum alloys, *comput. mater. Sci* **2013,** *67*, 1-10.
17. Yusef, M. G.; Solid State Physics, C2, *Ministry of Higher Education Press* **1989**, *23*, 34-44.
18. Burton, A. W. On the estimation of average crystallite size of zeolites from the Scherrer equation: a critical evaluation of its application to zeolites with on dimensional pore systems. *Microporous and Mesoporous Materials*, **2009**, *117*, 1-2. https://doi.org/10.1016/j.micromeso.2008.06.010
19. Prabhu, Y. T. X-ray analysis by Williamson-Hall and size-strain plot methods of ZnO nanoparticles with fuel variation. *World Journal of Nano Science and Engineering* **2014**, *12*(*2)*, 34-45. https://doi.org/10.4236/WJNSE.2014.41004
20. Nath, D.; Fouran, S.; Ratan, D. X-ray diffraction analysis by Williamson-Hall, Halder-Wagner and size-strain plot methods of CdSe nanoparticles-a comparative study. *Materials Chemistry and Physics* **2020**, *12*(*4)*, 55-67. https://doi.org/10.1016/j.matchemphys.2019.122021
21. Irfan, H.; Mohamed, R. K.; Anand, S.; Microstructural evaluation of CoAl2O4 nanoparticles by Williamson–Hall and size–strain plot methods. *Journal of Asian Ceramic Societies* **2018,** *6(1)*, 34-45. https://doi.org/10.1016/j.jmatprotec.2021.117063
22. Mohammed, H. M.; Kareem, A. J.; Study the effect of coating on the optical, insulation, thermal and structural properties of glass, *AIP Conference Proceedings* **2018**, *1*, 2437,

23. Suad, H. A.; Anaam, W. W.; Ebtisam, M. T.; Kareem, A. J.; Auday, H. S.; Tagreed, M. A. The study effect of weight fraction on thermal and electrical conductivity for unsaturated polyester composite alone and hybrid, *AIP Conf. Proc* **2018**, 020019-1–020019-5.
24. Raghavan, V. Material Science and Engineering, *5thed. New Delhi* **2010**, *414*, 12-23.
25. Jasim, K. A.; Mohammed, L. A. The partial substitution of copper with nickel oxide on the Structural and electrical properties of HgBa2Ca2Cu3-xNixO8+δ superconducting compound, *Journal of Physics: Conf. Series* **2018**, *1003*, 012071, 1-9. https://doi.org/10.1088/1742-6596%2F1003%2F1%2F012071
26. Bilal, A. O.; Sabah, J. F.; Kareem, A. J. Effect of Zn on the structural and electrical properties of high-temperature HgBa2Ca2Cu3O8+δ superconductor, *AIP Conference Proceedings* **2018,** *030047*, 23-45. http://dx.doi.org/10.1063/1.5039234
27. Wadia, K. M. Improvement of superconducting properties of Bi2Ba2Ca2Cu3O10+ δ Ceramic by prepared under different pressures, *Energy Procardia* **2019,** *157(23)*, 13-23. https://doi.org/10.1016/J.EGYPRO.2018.11.184
28. Maher, A. H.; Kareem, A. J.; Hussein, A. M. Synthesis and Comparative Analysis of Crystallite Size and Lattice Strain of Pb2Ba1.7Sr0.3Ca2Cu3O10+δ Superconductor, *Korean J. Mater. Res* **2022**, *32* (*2),* 12-23. https://doi.org/10.3740/MRSK.2022.32.2.66
29. Kareem, A. J.; Mohammed, A. N; Raghad, S. A. The Effect of Doping by Sr on the Structural, Mechanical and Electrical Characterization of La1Ba1-xSrx Ca2Cu4O8.5+δ, *Ibn Al-Haitham Jour. for Pure & Appl. Sci* **2014**, *27*(*1)*, 213-219. http://dx.doi.org/10.3390/su132212706
30. Hamadneh, I, K.; Hui, Y. W., Abd-Shukor, L. T Formation of Tl0.85Cr0.15Sr2CaCu2O7-delta superconductor from ultrafine co-precipitated powders, *Materials Letters* **2006**, *60(6)*, 734–736.
31. Shabana, H.; Mohammedb, L. A.; Hussein, H. S.; Jasim, K. A. The structural properties of Y1-XLaXBa4Cu7O15+ δ superconductor compound. Digest, *Journal of Nanomaterials and Biostructures* **2022,** *17(2)*, 519 – 525. https://doi.org/10.1039/c6sc05012c
32. Nawal, H. K.; Kareem, A. J. A Study of the Effectiveness of Tin on the Thermal Conductivity Coefficient and Electrical Resistance of Se60Te40-xSnx Chalcogenide Glass, *Ibn Al-Haitham Journal for Pure and Applied Sciences, Journal* **2023**, *12(3)*, 23-34. Doi.org/10.30526/36.1.2892.
33. Kareem, A. J.; Rihab, N. F. The Effects of Micro Aluminum fillers Epoxy resin on the thermal conductivity. *Ibn AL-Haithem 1st. International scientific conference* **2017**, *34(3)*, 45-55. http://dx.doi.org/10.1088/1742-6596/1003/1/012082
34. Choudhary, R.; Palai, R.; Sharma, S. Structural, Dielectric and Electri -cal Properties of Lead Cadmium Tungstate ceramics, *Materials Science and Engineering* **2000**, *77*, 235–240. https://doi.org/10.1016/S0022-3697%2800%2900217-1
35. Vilara, A.; Castro, B.; Rivas, A.; Mirab, J.; Rivasb, M. Study of the Dielectric Properties of the Perovskite $LaMn_{0.5}Co_{0.5}O_{3-\delta"}$, Z. *Anorg. Allg. Chem* **2005**, *631*, 2265-2272.
36. Adil, M. I. Effect Of Preparation Methods On The Structural, Mechanical and Electrical Properties Of $Bi_2Sr_2Ca_{2-x}Cd_xCu_3O_{10+\delta}$ System, *Master Thesis, University of Baghdad College Of Education For Pure Science Ibn- Al-Haitham Department of Physics* **2015**, *23(1)*, 23-33. http://dx.doi.org/10.13140/RG.2.2.18065.17765